



## Middle UV to near-IR spectrum of electron-excited SO<sub>2</sub>

Joseph M. Ajello,<sup>1</sup> Alejandro Aguilar,<sup>1,2</sup> Rao S. Mangina,<sup>1</sup> Geoffrey K. James,<sup>1</sup> Paul Geissler,<sup>3</sup> and Laurence Trafton<sup>4</sup>

Received 27 March 2007; revised 5 September 2007; accepted 12 November 2007; published 21 March 2008.

[1] We investigated the electron impact–induced fluorescence spectrum of SO<sub>2</sub> to provide excitation cross sections for modeling Io’s emission spectrum and analyzing Cassini Imaging Science Subsystem observations. The electron-excited middle-ultraviolet visible optical near-infrared (VOIR) emission spectrum of SO<sub>2</sub> gas was generated in the laboratory and studied from 2000 to 11,000 Å at a resolution of  $\Delta\lambda \sim 2.5$  Å full width at half maximum (FWHM). The VOIR laboratory spectrum longward of 6000 Å consists entirely of S I, II and O I<sub>2</sub> II multiplets for electron impact energies above  $\sim 15$  eV. Between 2000 and 6000 Å, we find previously identified molecular bands from both SO and SO<sub>2</sub>. This work represents a significant improvement in spectral resolution over our earlier work done at 18 Å FWHM. From a measurement of the medium-resolution spectrum, we provide detailed 25- and 100-eV emission cross sections for spectral features from 2000 to 11,000 Å. On the basis of these data, we suggest future ground-based and satellite telescopic observations in the VOIR that are of promise for understanding Io’s atmosphere.

**Citation:** Ajello, J. M., A. Aguilar, R. S. Mangina, G. K. James, P. Geissler, and L. Trafton (2008), Middle UV to near-IR spectrum of electron-excited SO<sub>2</sub>, *J. Geophys. Res.*, 113, E03002, doi:10.1029/2007JE002921.

### 1. Introduction

[2] Observations of the Jupiter system by NASA spacecrafts occur periodically as Jupiter is a necessary target for a gravitational assist trajectory to the outer solar system (e.g., the Cassini and New Horizons missions). Jupiter, as the largest and most massive giant planet, is also a scientific destination (Galileo and JUNO). Active magnetospheres are coupled to the ionospheres of the giant planets’ systems and contribute to particle-excited aurora and airglow. Trapped particle impact on a satellite atmosphere can result in global excitation within both day and night hemispheres. For Io, having a volcanically generated SO<sub>2</sub> atmosphere, dissociative excitation by the magnetospheric Jovian plasma torus results in excited SO, S and O, in addition to excited SO<sub>2</sub> and ions, all of which emit radiation. It is believed that the bulk of Io’s atomic emission is powered by electron excitation of neutral S and O directly, rather than by the electron dissociative excitation of SO<sub>2</sub> [Ballester *et al.*, 1996]. There is an evidence, however, that both processes contribute to the Io emission spectrum: (1) *Oliveresen et al.* [2001] indicate that short-term fluctuations in the O I 6300 Å intensity is the evidence for a high-energy nonthermal plasma tail ( $\sim 30$  eV) for a one step process,

and (2) *Ballester* [1998] indicates that neither electron excitation of O I nor electron dissociative excitation of SO<sub>2</sub> alone by plasma electrons can explain the Hubble Space Telescope (HST) or International Ultraviolet Explorer (IUE) observations.

[3] Scientific spectroscopic studies of Jupiter and its satellites are performed by remote sensing instruments scanning from the UV to IR. The closest approach to Jupiter by the New Horizons (NH) spacecraft occurred on 28 February 2007 and during the encounter, NH monitored the Io’s atmosphere (<http://sse.jpl.nasa.gov/missions/profile.cfm?Sort=Alpha&Target=Pluto>). NH is equipped with instruments that are sensitive to the visible and near IR, the Ralph instrument (visible and near IR imager and spectrometer), the Long Range Reconnaissance Imager instrument, and the Multicolor Visible Imaging Camera, and collected data in the present wavelength range. Preliminary results have been recently presented by *Retherford et al.* [2007a, 2007b, 2007c]. There are also dedicated earth based satellite observations with HST and IUE.

[4] We have been supporting the NASA missions engaged in Io monitoring through a laboratory program that measures electron impact–induced spectra and derives cross sections of SO<sub>2</sub> in the UV [Vatti Palle *et al.*, 2004; Ajello *et al.*, 1992a] and Visible [Ajello *et al.*, 1992b, 2002] and atomic O in the UV [Noren *et al.*, 2001; Johnson *et al.*, 2003]. Our atomic and molecular data have been used most recently in the analysis of the Galileo Solid State Imaging observations of Io [Geissler *et al.*, 1999], Cassini spacecraft observations of Io by the Imaging Science Subsystem (ISS) [Porco *et al.*, 2003; Geissler *et al.*, 2004], and the Ultraviolet Imaging Spectrograph [Esposito *et al.*, 2005]. The ISS

<sup>1</sup>Jet Propulsion Laboratory, California Institute of Technology, Pasadena, California, USA.

<sup>2</sup>Now at Advanced Light Source, Lawrence Berkeley National Laboratory, Berkeley, California, USA.

<sup>3</sup>U.S. Geological Survey, Flagstaff, Arizona, USA.

<sup>4</sup>Department of Astronomy, University of Texas at Austin, Austin, Texas, USA.

is equipped with 15 filter combinations that span the wavelength range of 2350–11,000 Å. From the data acquired during the Jupiter Millennium encounter, *Geissler et al.* [2004] performed a detailed comparison of the laboratory SO<sub>2</sub> spectra with the Cassini observations, and inferred that a mixture of gases contribute to the equatorial glow. The equatorial glows were particularly bright in the near ultraviolet wavelengths (2300–5000 Å) filters UV1, UV2, UV3, and B11. On the basis of the laboratory work of *Ajello et al.* [1992a, 1992b, 2002] the relative emission intensities within each band pass confirm the presence of molecular SO<sub>2</sub> in the Io atmosphere. Most of the filters from the blue to the near IR (5000–12,000 Å) show substantial emission intensities. The laboratory work of *Ajello et al.* [2002] used in the comparison only covered the wavelength range of 2000–6000 Å. In this work we expand our wavelength coverage to include the entire range of 2000–11,000 Å using our newly acquired laboratory spectroscopic instrumentation that closely matches the Cassini ISS wavelength capability. This added coverage is the first study of SO<sub>2</sub> from the UV, visible, optical to near IR, hereinafter referred to as the VOIR, which is needed to confirm the model analysis of *Geissler et al.* [2004].

[5] Previous work in this field by other laboratories includes the electron impact work of *Miller and Becker* [1987]. They studied the emission spectrum of SO<sub>2</sub> from 2000 to 8000 Å (with little sensitivity above 6000 Å and no mention of the strong multiplet at 7773.4 Å) from emission thresholds to 500 eV and noted the two major molecular emission features: MUV1 middle ultraviolet (MUV1) from 2400 to 2650 Å and MUV2 from 2500 to 4600 Å at a resolution of 20 Å full width at half maximum (FWHM). Detailed study of MUV1 and MUV2 was carried out later by *Ajello et al.* [1992b] from emission thresholds to 1 keV. The O I, II and S I, II emission features from dissociative excitation were found to be weak in comparison to the integrated cross section of the molecular emissions of MUV1 and MUV2. A few years later *Kiehling et al.* [2001] investigated the VOIR spectrum from 3800 to 8000 Å produced by proton impact on SO<sub>2</sub>. *Kiehling et al.* found the molecular features to be weak in comparison to the scores of O I, II and S I, II atomic Rydberg series. The strongest feature was determined to be O I 7773.4 Å. Another important cross section measurement of SO<sub>2</sub> was made by *Kedzierski et al.* [2000]. *Kedzierski et al.* measured the electron excitation cross section of atomic O metastable fragments in the <sup>1</sup>S state at 150 eV to be  $2.2 \times 10^{-18}$  cm<sup>2</sup>. Our work will be the first at medium spectral resolution (resolving power of about 3000) and over the entire wavelength range of the VOIR. The laboratory instrument, which is an imaging spectrometer, has high sensitivity to weak atomic features and can measure weak cross sections of the order of  $10^{-20}$ – $10^{-21}$  cm<sup>2</sup>.

[6] Astronomical studies have shown the presence of atomic and molecular emission structure in the ground-based and satellite-based spectroscopic studies of Io. The morphology of the emissions show (1) bright equatorial UV glows that are dominated by molecular SO<sub>2</sub> and (2) limb emissions encircling Io, observed at visible to near IR wavelengths, suggestive of emissions from atomic species [*Wolven et al.*, 2001; *Feaga et al.*, 2002; *Retherford et al.*, 2000, 2003; *Geissler et al.*, 2004]. For example, high-

resolution ground-based studies have confirmed the presence of atomic O emissions from O(<sup>1</sup>D) at 6300 Å [*Oliveresen et al.*, 2001]. The emission arises from a combination of electron impact excitation processes. Both direct electron impact excitation of atomic O and dissociative excitation of molecular SO<sub>2</sub> and SO could contribute to the observed morphology. Additional O I forbidden emission lines are expected at 5577, 6300, and 6364 Å. Strong dipole-allowed O I lines are expected at 7774 and 8446 Å and their dominant cascade channels for UV emissions are 1356 and 1304 Å, respectively. The UV emissions have been extensively studied by HST/STIS (Hubble Space Telescope Imaging Spectrograph) [*Roesler et al.*, 1999; *Retherford et al.*, 2000; *Wolven et al.*, 2001; *Feaga et al.*, 2002]. The UV observations show an upper atmosphere of O and S that is globally distributed. Model calculations of Io's lower atmosphere have shown that SO<sub>2</sub> is the dominant species in the dayside atmosphere while O<sub>2</sub> and SO (dominant one) are the major species in the nightside atmosphere [*Wong and Smyth*, 2000]. The dynamics of Io's atmosphere depend on the interaction of the neutral gases in Io's atmosphere, including the volcanic plumes, and their interaction with the corotating plasma torus of sulfur and oxygen ions and electrons. *Saur et al.* [2000] have explained Io's aurora as the interaction of an ionospheric current with the ambient neutral species. Monte Carlo models of the Io airglow and aurora that make use of the cross sections presented here in order to calculate emission intensities have been developed by *Bhardwaj and Marykutty* [1999a, 1999b].

[7] In this paper we describe (1) the laboratory instrumentation and the spectra from the VOIR instrument, (2) the cross sections of SO<sub>2</sub> at 25 and 100 eV based on comparing the O I 7773.4 Å multiplet emission (excited directly from molecular dissociation of SO<sub>2</sub>) and the well-known H<sub>α</sub> at 6563 Å (from the dissociation of molecular H<sub>2</sub>), and (3) likely astronomical spectral observations of promise by HST and ground based telescopes equipped with slit spectrographs.

## 2. Experimental Apparatus

[8] The VOIR instrument consists of a visible to near infrared imaging spectrometer operating in air in conjunction with an electron impact collision chamber under vacuum. A schematic of the apparatus is shown in Figure 1. The spectrometer and collision chamber are vacuum isolated by a quartz window. A magnetically collimated beam of electrons (with selected energy within the range of 10–1000 eV) is crossed with a beam of gas formed by a capillary array under optically thin conditions at a background pressure of  $1 \times 10^{-4}$  torr. The electron impact-induced fluorescence spectrum is observed at 90° emission angle using a Spectra Pro 0.5 m spectrometer which has the capability of achieving resolving power of 10,000 at 5000 Å, when using a 50 μm entrance slit. The spectrometer is equipped with a Princeton Instruments liquid nitrogen cooled charge-coupled device (CCD) detector array of 1340 pixels wide and 400 pixels tall (each pixel is 20 μm<sup>2</sup>). The wavelength response of the detector is calibrated using standard deuterium and tungsten sources from 2000 to 11,000 Å.

[9] There are three gratings on the instrument: (1) 1800 grooves/mm: 2500 Å blaze wavelength (16.67 Å/mm),

## EXPERIMENTAL APPARATUS

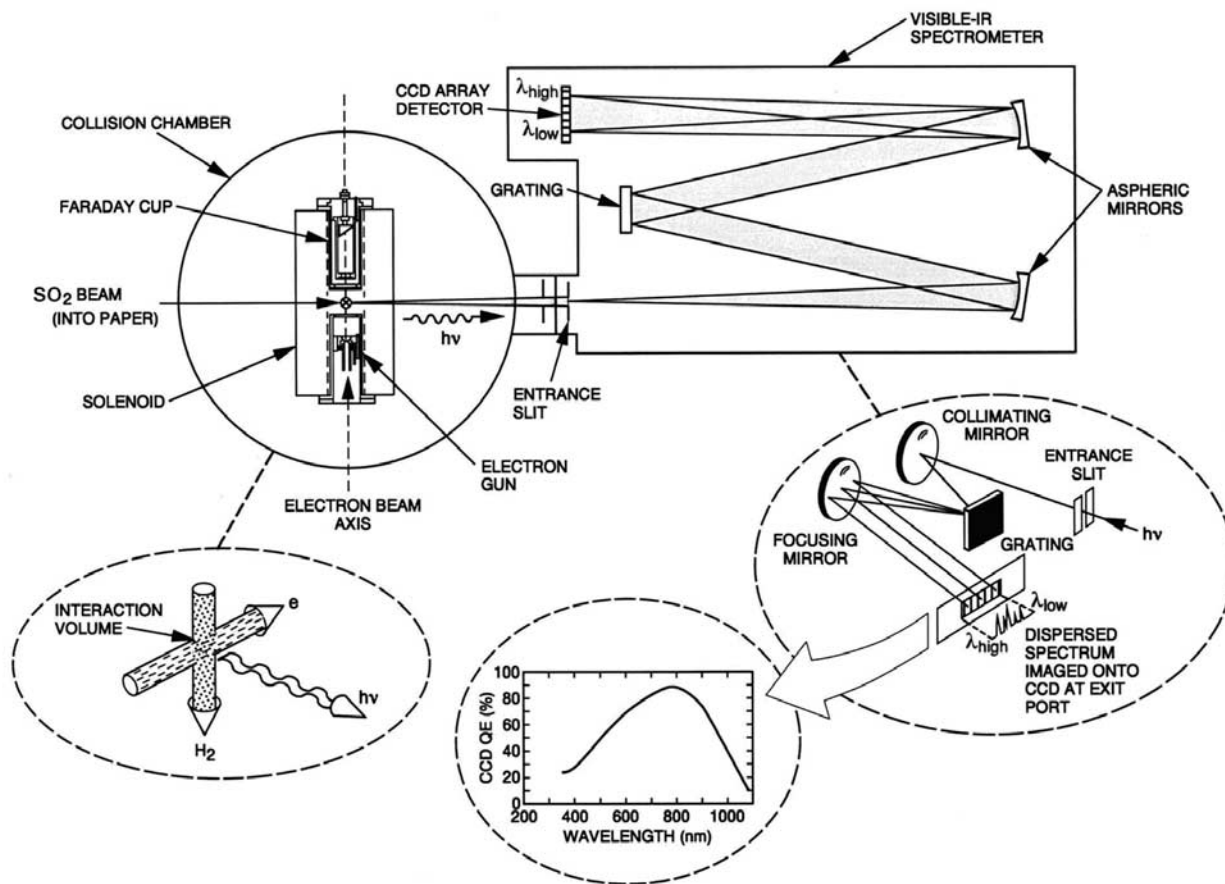


**Figure 1.** Schematic diagram of the visible optical near-infrared (VOIR) experimental apparatus, showing the collision chamber, the interaction region, a schematic calibration curve, the Czerney-Turner optics of the grating turret, and the two mirrors of the spectrometer.

(2) 1800 grooves/mm: 5000 Å blaze wavelength (16.67 Å/mm), and (3) 1200 grooves/mm: 7500 Å blaze wavelength (11.11 Å/mm). Order sorting filters are used for gratings 2 and 3 with low wavelength cutoffs of 3200 Å and 5900 Å, respectively. The three overlapping wavelength ranges for the spectrometer are 2000–3800 Å using grating 1, 3600–8000 Å using grating 2, and 6000–11,000 Å using grating 3. The full range of a grating is covered during an experiment by rotating the grating in predetermined small steps. At a given grating position the wavelength range captured by the detector array varies from 200 Å to 250 Å depending upon the grating and slit sizes used.

[10] Spurious signals in CCD arrays due to cosmic ray hits are common. These hits cause an increase in charge in one or more pixels which are indistinguishable from the arrival of signal photons. In our experience, an active detector exposed for a few minutes might have nearly two dozen cosmic ray hits. Since the location of the cosmic ray hits within the chip is random in space and time, a common algorithm is used to remove them without altering the photosignal [Aguilar *et al.*, 2008]. This is achieved by collecting several frames under the same conditions and removing the counts due to the cosmic ray hits by compar-

ing the corresponding pixels in different image frames. In this process the algorithm rejects those with aberrantly large values. In the present experiment, 10 frames of 3 min each were collected for each grating position. The wavelength overlap for consecutive grating positions was typically 4 Å.

[11] We have measured the instrument resolution by studying one of the fine structure lines of the SI 9213 Å multiplet  $4s\ ^5S-4p\ ^5P$  measured with grating 3. In Figure 2 we show the instrument performance for several slit widths, including the 150  $\mu\text{m}$  slit setting for this study (2.5 Å FWHM). Owing to the larger grating constant (smaller groove density) the FWHM obtained with grating 3 is larger than with grating 2 (1.5 Å FWHM) for the same slit width. The instrument is capable of achieving high resolution ( $\lambda/\Delta\lambda > 10,000$ ) with entrance slit width below 50  $\mu\text{m}$  in the VOIR for both the gratings. For example, we have measured the fine structure of the O I (7773.4 Å)  $^5S^o-^5P$  multiplet using grating 2. The fine structure features at 7771.94 Å ( $^5S^o_2-^5P_1$ ), 7774.17 Å ( $^5S^o_2-^5P_2$ ) and 7775.39 Å ( $^5S^o_2-^5P_3$ ) for this multiplet are shown in Figure 3. The instrument resolves the three fine structure lines with 10- to 50- $\mu\text{m}$  slit settings. The relative intensities of these spectral features are

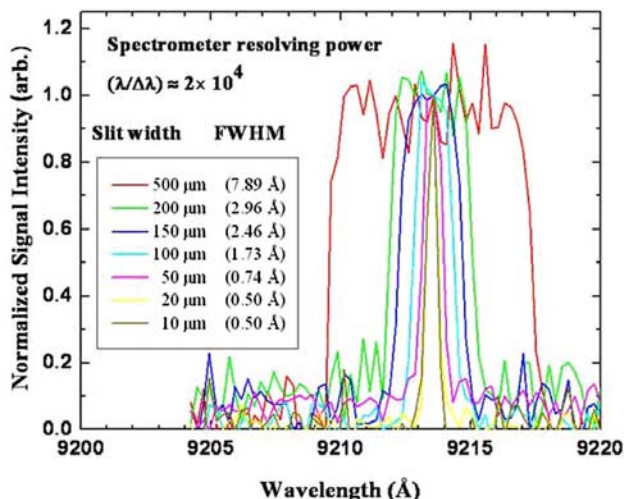


**Figure 2.** Instrumental slit function as measured by placing the central wavelength on one of the fine structure lines of the SI 9213 Å multiplet  $4s^5S-4p^5P$  using grating 3. The full width half maximum (FWHM) is given for various entrance slit settings from 10 to 500 μm. The best resolving power ( $R$ )  $\lambda/\Delta\lambda \approx 2 \times 10^4$  was obtained with a 10-μm entrance slit width. The  $R$  at 150 μm used in the present measurements is about  $0.4 \times 10^4$ .

compared with their values given in the NIST standard database; the agreement is excellent.

[12] The spectrometer was calibrated with deuterium and tungsten blackbody spectral Irradiance Lamps over the spectral range of 2000–12,000 Å spanned by the three gratings. We show in Figure 4 the relative inverse sensitiv-

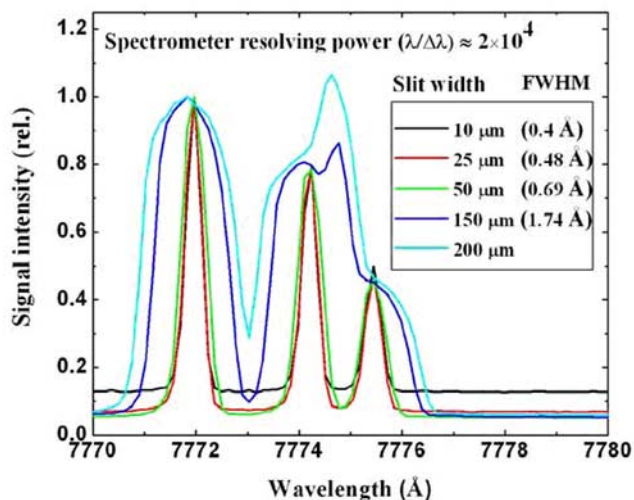


**Figure 3.** Instrument performance in measuring the O I fine structure features at 7771.94 Å ( $^5S_2-^5P_1$ ), 7774.17 Å ( $^3S_2-^5P_2$ ), and 7775.39 Å ( $^5S_2-^5P_3$ ) for grating 2. The instrument is capable of resolving the three fine structure lines less than 1 Å separation for 10- to 50-μm slit settings. The best resolving power ( $R$ )  $\lambda/\Delta\lambda \approx 2 \times 10^4$  was obtained with a 10-μm entrance slit width. The  $R$  at 150 μm used in the present measurements is about  $0.5 \times 10^4$ .

ities ( $S^{-1}$ , which is defined as the input standard blackbody spectrum irradiance divided by the measured output spectrum of spectrometer) for the 5000 Å blaze with grating 2 and 7500 Å blaze with grating 3. The inverse sensitivity of grating 1 is not shown in Figure 4 as it is similar to the grating reported earlier by us [Terrell *et al.*, 2004].

[13] The absolute calibration of the optical system for SO<sub>2</sub> gas at 25 eV and 100 eV electron impact energies was based on the known emission cross sections of H<sub>α</sub> at 25 eV and 100 eV electron impact energies in a static gas experiment. Although the presence of 100 eV electrons is unlikely in the Io atmosphere the experimental cross sections of 100 eV were measured for comparison of atomic and molecular emissions of SO<sub>2</sub> and also as a reference datum for future. Moreover, 100 eV is the standard energy at which most of the cross sections for several species are reported and compared in the literature. Karolis and Harting [1978] measured the electron impact dissociation cross section of H<sub>2</sub> from threshold 15.6 eV and 100 eV. The cross sections for H<sub>α</sub> at 25 eV and 100 eV reported by them are  $0.54 \times 10^{-18}$  and  $0.93 \times 10^{-18}$  cm<sup>2</sup>,

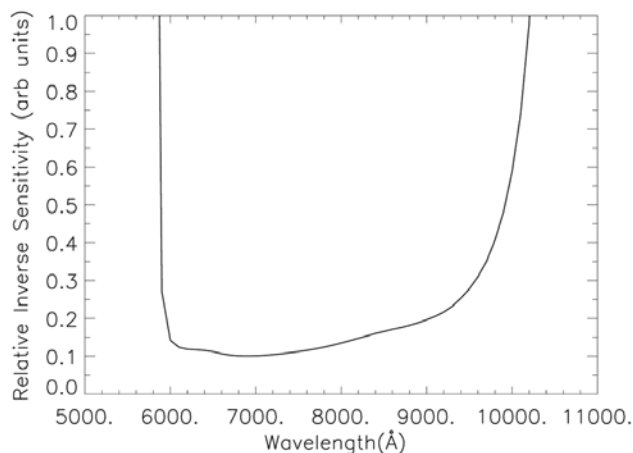
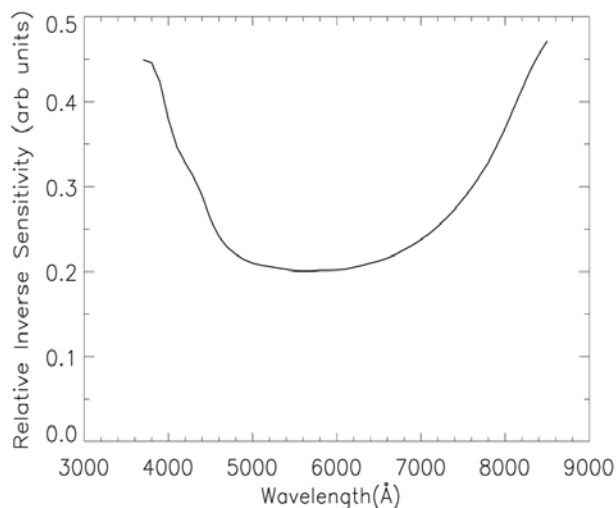


**Figure 4.** Inverse sensitivity of grating 2 (top) and 3 (bottom) as determined from a blackbody spectral irradiance lamp with an emitting surface in the shape of an integrating sphere.

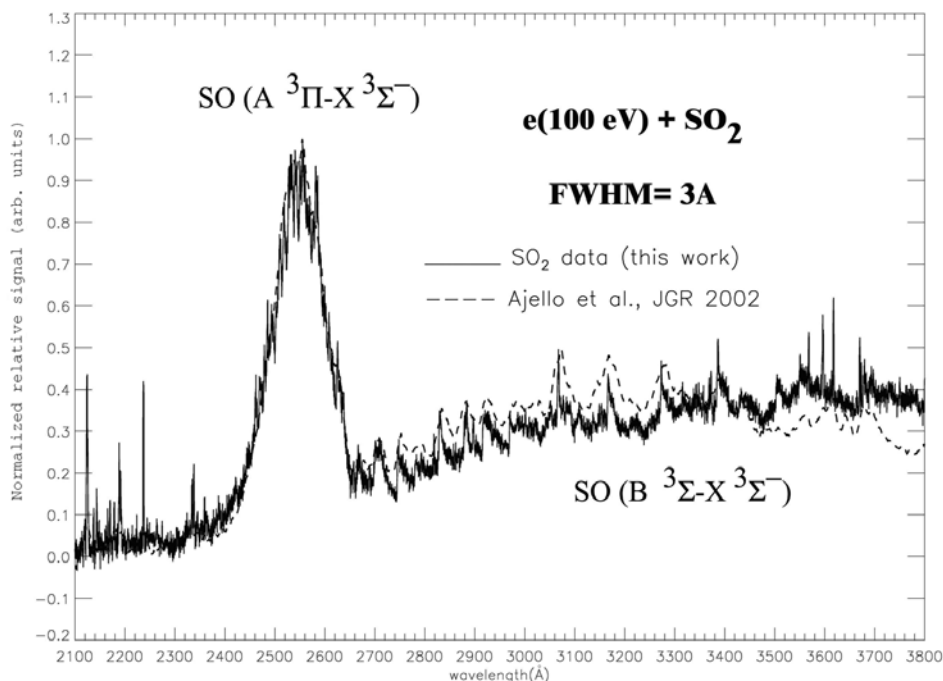


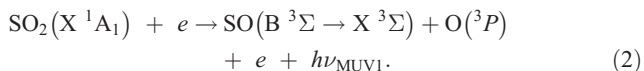
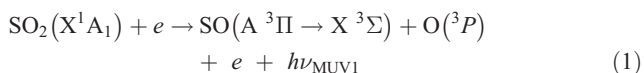
**Figure 5.** Calibrated electron impact–induced fluorescence spectrum (2100–3800 Å) of SO<sub>2</sub> at 100-eV electron impact energy (solid line) compared to the spectrum of *Ajello et al.* [2002] (dashed line) at 2 Å FWHM. Two of the SO band systems are identified. The cross section value of SO band (B <sup>3</sup>Σ → X <sup>3</sup>Σ) around 2560 Å at 100 eV is  $21 \times 10^{-19} \text{ cm}^2$  [*Ajello et al.*, 2002].

respectively. A static gas comparison of the intensity of the atomic oxygen multiplet at 7773.4 Å (integrated over the three fine structure lines) with the intensity of H<sub>α</sub> yielded the 25 eV and 100 eV emission cross sections for the electron impact dissociative emission cross section of SO<sub>2</sub>. The two emission cross sections were found to be  $0.39 \times 10^{-18} \text{ cm}^2$  and  $4.2 \times 10^{-18} \text{ cm}^2$ , respectively. The comparison of the two multiplets was conducted under similar conditions with  $\sim 100 \mu\text{-amps}$  electron beam current and  $1 \times 10^{-4}$  torr gas pressure. Karolis and Harting compare their results for the emission cross section to the work of two other authors in different laboratories. We base the uncertainty of our absolute calibration primarily upon the 20% variation of the H<sub>α</sub> cross sections for the three experiments cited by Karolis and Harting. A recent review of the H<sub>α</sub> cross sections from the dissociative excitation of H<sub>2</sub> by *Lavrov and Pipa* [2002] is in good agreement ( $\sim 10\%$ ) with the *Karolis and Harting* [1978] result. Additional uncertainties of the O I (7774 Å) absolute cross section can be traced to the 10% correction of the two gas pressures using a Varian Bayard-Alpert UHV gauge tube, to the variation of electron beam current, and to the stability of the gas pressure during the spectral scan of 15%. The relative uncertainty of the instrument calibration is 10% over the range of each grating. The root-sum-square uncertainty of the absolute cross sections is 30%.

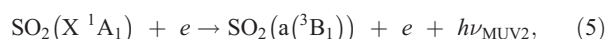
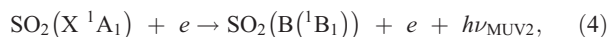
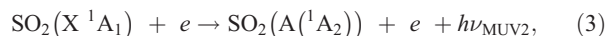
### 3. Experimental Results

[14] The electron impact–induced fluorescence spectrum of SO<sub>2</sub> at 100 eV electron impact energy from 2000 to 11,000 Å was measured in three separate segments using

gratings 1, 2, and 3. The respective spectra are shown in Figures 5, 6, and 7. Figure 5 shows the VOIR spectrum from 2100 to 3800 Å at 100 eV electron impact energy. An excellent agreement between the earlier work of *Ajello et al.* [2002] and the present work for the same wavelength range is shown in Figure 5. The two broad molecular structures centered near 2550 Å and 3600 Å have been previously labeled MUV1 (2385–2670 Å) and MUV2 (2670–6000 Å) and thoroughly discussed by *Ajello et al.* [1992b]. In brief, the two excitation processes for MUV1 are as follows:



Many excitation processes contribute to MUV2. The spectrum appears as a quasicontinuum with underlying vibrational structure. The molecular structure is complicated, with the excited molecules being SO<sub>2</sub>, SO or SO<sub>2</sub><sup>+</sup>. The excitation processes are as follows:



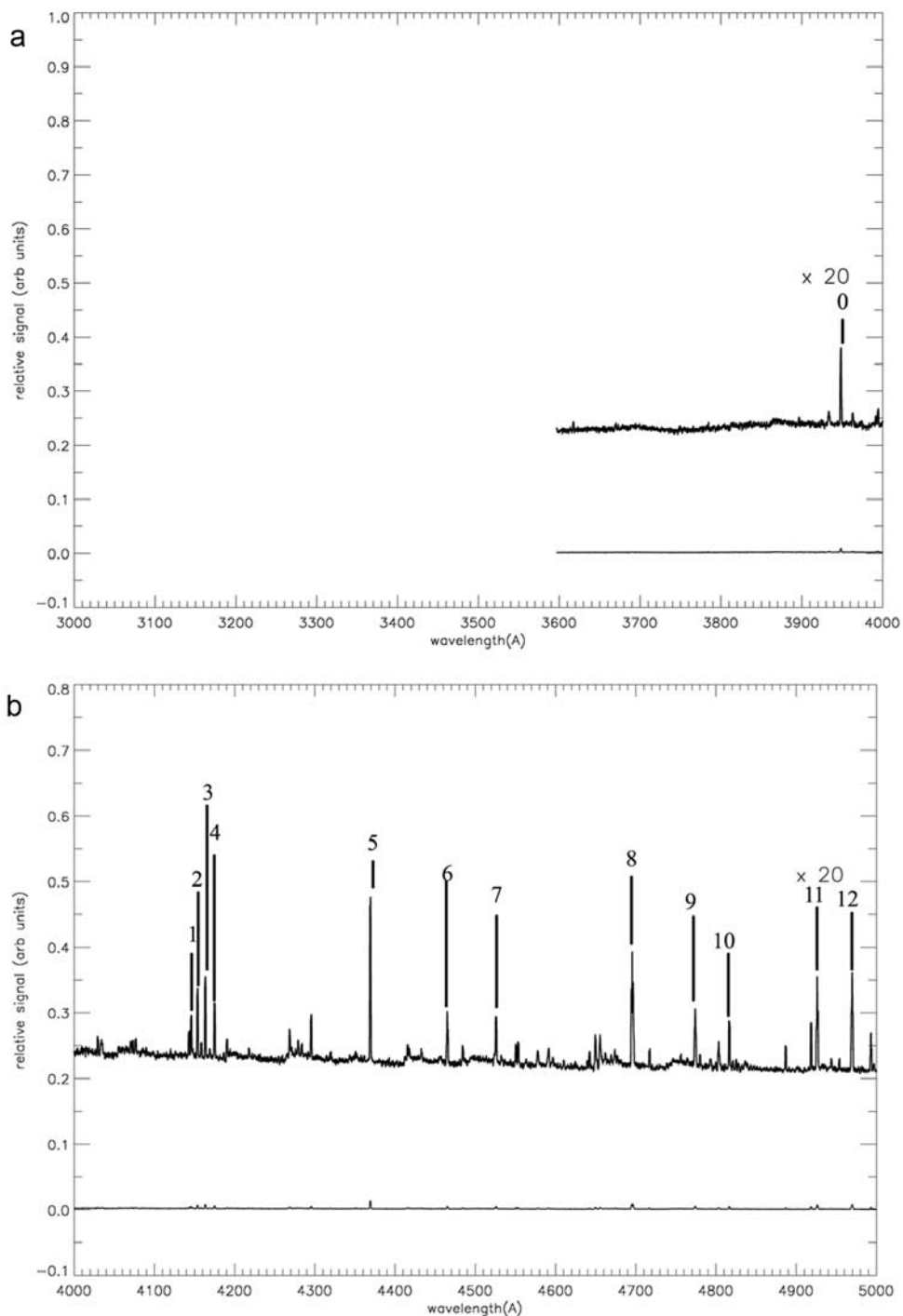


**Figure 6.** Calibrated electron impact–induced fluorescence spectrum (3600–6000 Å) of SO<sub>2</sub> at 100-eV electron impact energy: (a) 3600–4000 Å, (b) 4000–5000 Å, and (c) 5000–6000 Å from grating 2. The strongest features, labeled 0–32, are identified by species and multiplet in Table 1. The relative heights of lines shown among the subplots (Figures 6a–6c) are with respect to feature 48 in Figure 7.

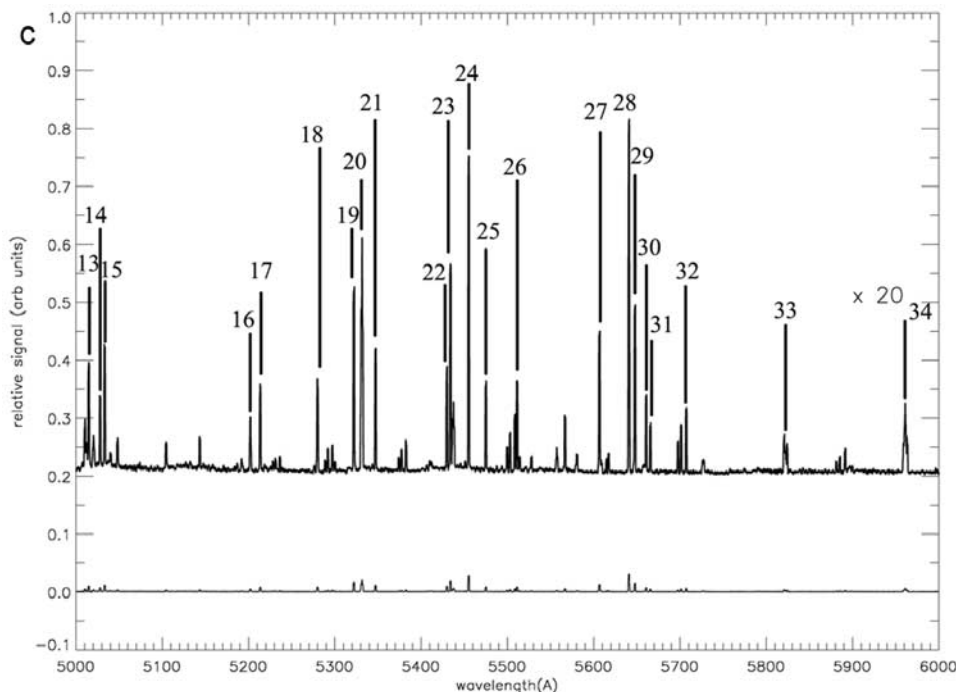
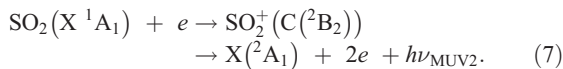
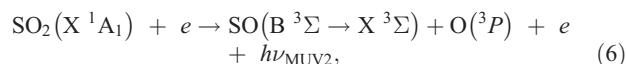


Figure 6. (continued)



The cross sections for molecular emissions from MUV1 and MUV2 at 98 eV have been given by *Ajello et al.* [2002] as  $21 \times 10^{-19} \text{ cm}^2$  and  $100 \times 10^{-19} \text{ cm}^2$ , respectively. The atomic multiplet VOIR emission cross sections found longward of 3900 Å were estimated to have a cross section of  $4 \times 10^{-18} \text{ cm}^2$  at 98 eV. It is our goal in this paper to study the atomic emissions in more detail.

[15] The atomic emissions are located over the wavelength range from 3900 to 11,000 Å. In the region of 3900–6000 Å the atomic multiplets lie on top of the MUV2 continuum. Beyond 6000 Å we find no evidence of further molecular structures. We show the grating 2 portion of the 100 eV VOIR spectrum from 3600 to 6000 Å in Figures 6a–6c. The 25 and 100 eV cross sections for the features labeled 0–32 in Figures 6a–6c are listed in Table 1. Features 33 and 34 of Figure 6c were again measured using grating 3 and are shown as Features 1 and 3 in Figure 7a and their cross sections are listed in Table 2. Most of the multiplets measured by grating 2 are O II and S II. Ionic features have a threshold above 25 eV. The atomic spectrum appears to be very weak at 25 eV and is composed of only the few O I and S I lines listed in Table 1. The strongest atomic features in the grating 2 region at 100 eV electron impact energy are features with numbers 20, 24, and 28. Feature 20 at 5330.74 Å is O I  $3p^5P-5d^5D$  with a cross section of  $7.16 \times 10^{-20} \text{ cm}^2$ . This feature ultimately populates the  $3s^5S$  quintet levels that contribute to the O I

1356 Å UV airglow feature of Io [*Vatti Palle et al.*, 2004] by the cascade transition multiplet  $3s^5S-3p^5P$  at 7773.4 Å, which was observed in the grating 3 spectrum (Figure 7c). The other two strongest multiplets (features 24 and 28) in Figure 6c are S II multiplets. Feature 24 at 5453.83 Å is the transition  $4s^2P-4p^4D$  with a cross section of  $6.93 \times 10^{-20} \text{ cm}^2$ . Feature 28 at 5640.33 Å is the transition  $3d^4F-4p^4D$  with a cross section of  $6.68 \times 10^{-20} \text{ cm}^2$ . These levels are cascade transitions to upper levels of the strong extreme ultraviolet (EUV) lines found in the Io torus, although in the torus the plasma sulfur spectrum consists of electron-excited S ions only. For example, the S II transition  $3d^2D-3p^2D$  at 957.88 Å is a strong Io torus feature measured by the Cassini UVIS (Ultraviolet Imaging Spectrograph). The adiabatic threshold for the S II multiplet from SO<sub>2</sub> is 37.7 eV and electrons of this energy are unlikely to be found in the Io atmosphere. This feature will not be in the Io atmosphere spectrum in the VOIR, whereas the O I multiplet has an adiabatic threshold of 18.8 eV and could be excited by the thermal tail of the Io electron distribution [*Oliveresen et al.*, 2001].

[16] The most intense part of the VOIR spectrum at 100 eV electron impact energy was measured with grating 3 shown in Figures 7a–7f with 1000 Å segments in each subfigure. Figure 7 spans the wavelength range from 5600 to 11,000 Å. The approximately 100 most intense atomic and ionic emission features are identified in Table 2 with their cross section values at both 25 eV and 100 eV. Unidentified multiplets in the NIST database are located by their experimental wavelengths and are denoted by a question mark next to the NIST identification for not knowing their transitions. About a dozen measured features that are not found in the NIST database are marked with footnotes in Table 2. The 25 eV spectrum is devoid of ionic features. The three most intense atomic multiplets are

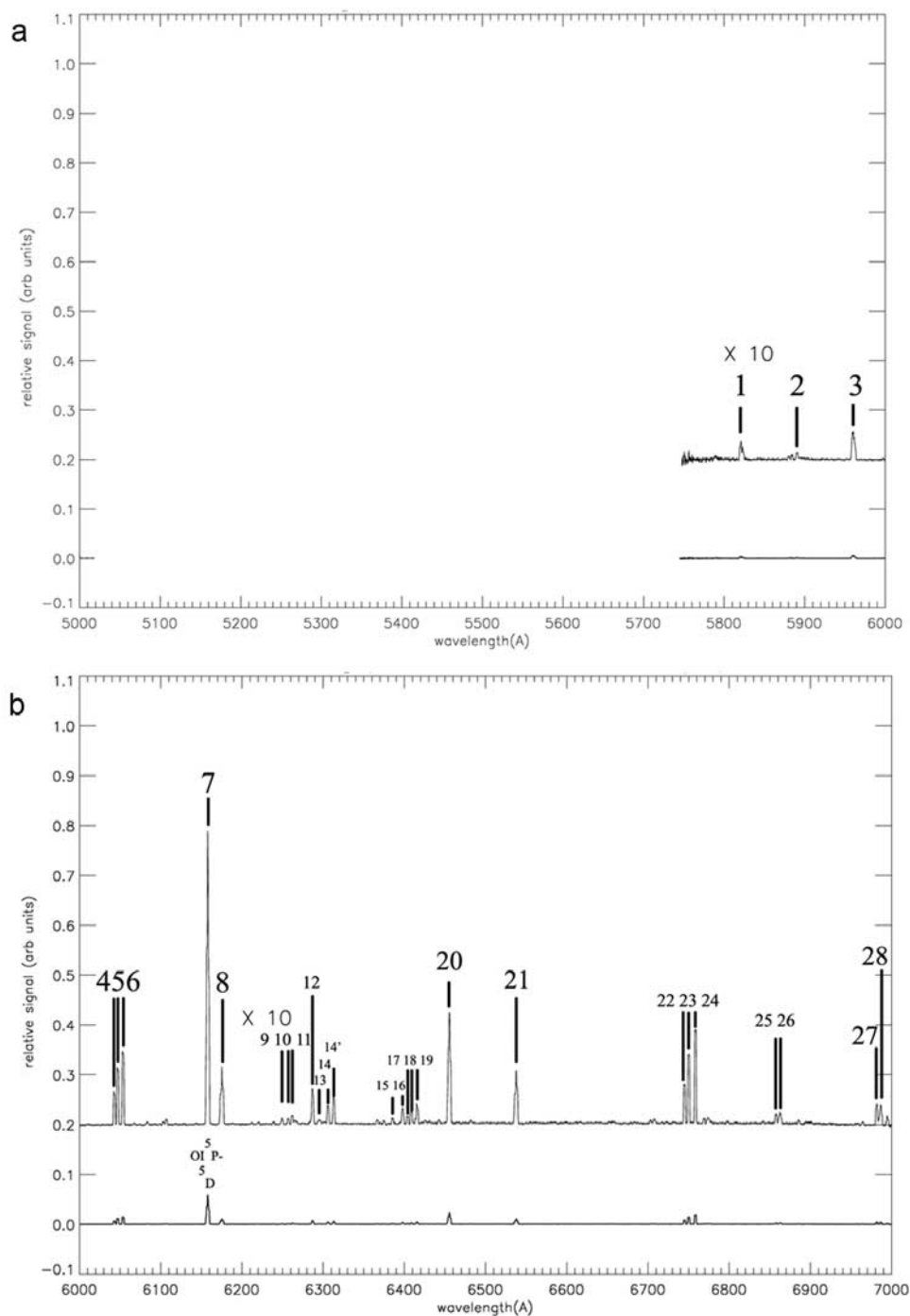


**Figure 7.** Calibrated electron impact-induced fluorescence spectrum (5600–11,000 Å) of SO<sub>2</sub> at 100-eV electron impact energy: (a) 5600–6000 Å, (b) 6000–7000 Å, (c) 7000–8000 Å, (d) 8000–9000 Å, (e) 9000–10,000 Å, and (f) 10,000–11,000 Å from grating 3. The strongest features are labeled 1–93 and are identified by species and multiplet in Table 2. The relative heights shown among the subplots (Figures 7a–7f) are with respect to feature 48.

feature numbers 40 at 7773.4 Å (a blend of 7771.94, 7774.17, and 7775.39 Å), 48 at 8446.36 Å, and 60 at 9212.86 Å, all three arising from neutral atoms. We recognize these features as important cascade emissions contributing to the

UV spectra of O and S. Feature numbers 40 and 48 are the atomic O transitions  $3s\ ^5S-3p\ ^5P$  and  $3s\ ^3S-3p\ ^3P$ , respectively. The 7773.4 Å feature has a cross section of  $4.20 \times 10^{-18}\ \text{cm}^2$  at 100 eV. The lower state of this

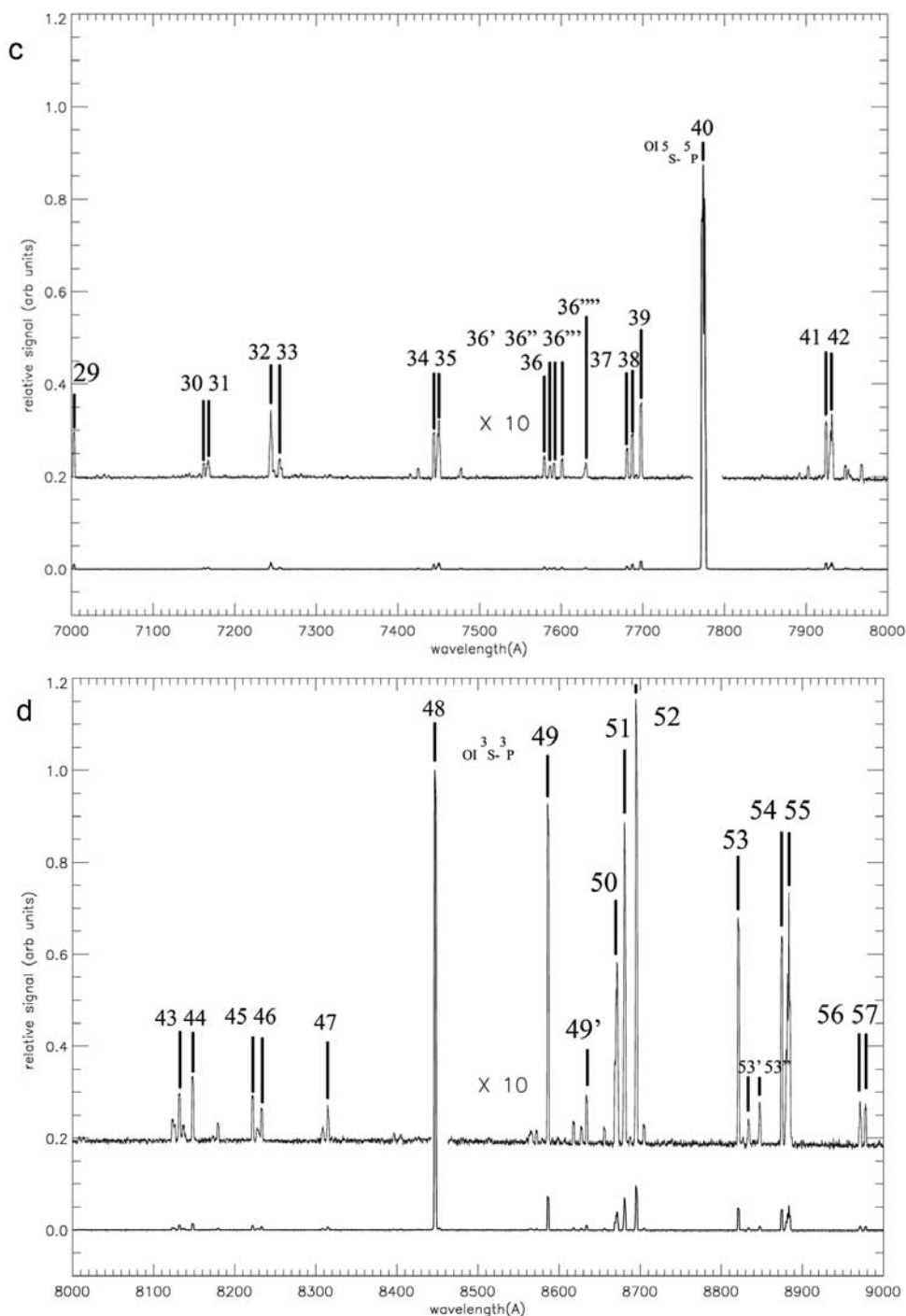


Figure 7. (continued)

transition,  $3s\ ^5S$ , is the upper state of the 1356 Å multiplet  $2p\ ^3P-3s\ ^5S$ . The cross section of the 1356 Å multiplet at 100 eV was estimated to be  $2.1 \pm 1 \times 10^{-18}\text{ cm}^2$  [Vatti Palle *et al.*, 2004]. Similarly, feature 48 at 8446.7 Å has a cross section of  $2.60 \times 10^{-18}\text{ cm}^2$  at 100 eV. The lower state of this transition,  $3s\ ^3S$ , is the upper state of the 1303.4 Å multiplet  $2p\ ^3P-3s\ ^3S$ . The cross section of the 1303.4 Å multiplet at 100 eV was found to be  $2.3 \pm 0.5 \times 10^{-18}\text{ cm}^2$

[Vatti Palle *et al.*, 2004]. Within the experimental error of the two experiments the two UV multiplets formed by dissociative excitation are found to be dominated by the cascading as compared to the direct excitation to the  $3s\ ^3,5S$  states.

[17] The strong SI multiplet at 9212.9 Å arises from the transition  $4s\ ^5S-4p\ ^5P$ . The  $4s\ ^5S$  is the upper state to an intense UV multiplet at 1914.70 Å ( $3p\ ^3P_1-4s\ ^5S$ ) with a lifetime of 52 μs. Ajello *et al.* [1992a] measured this

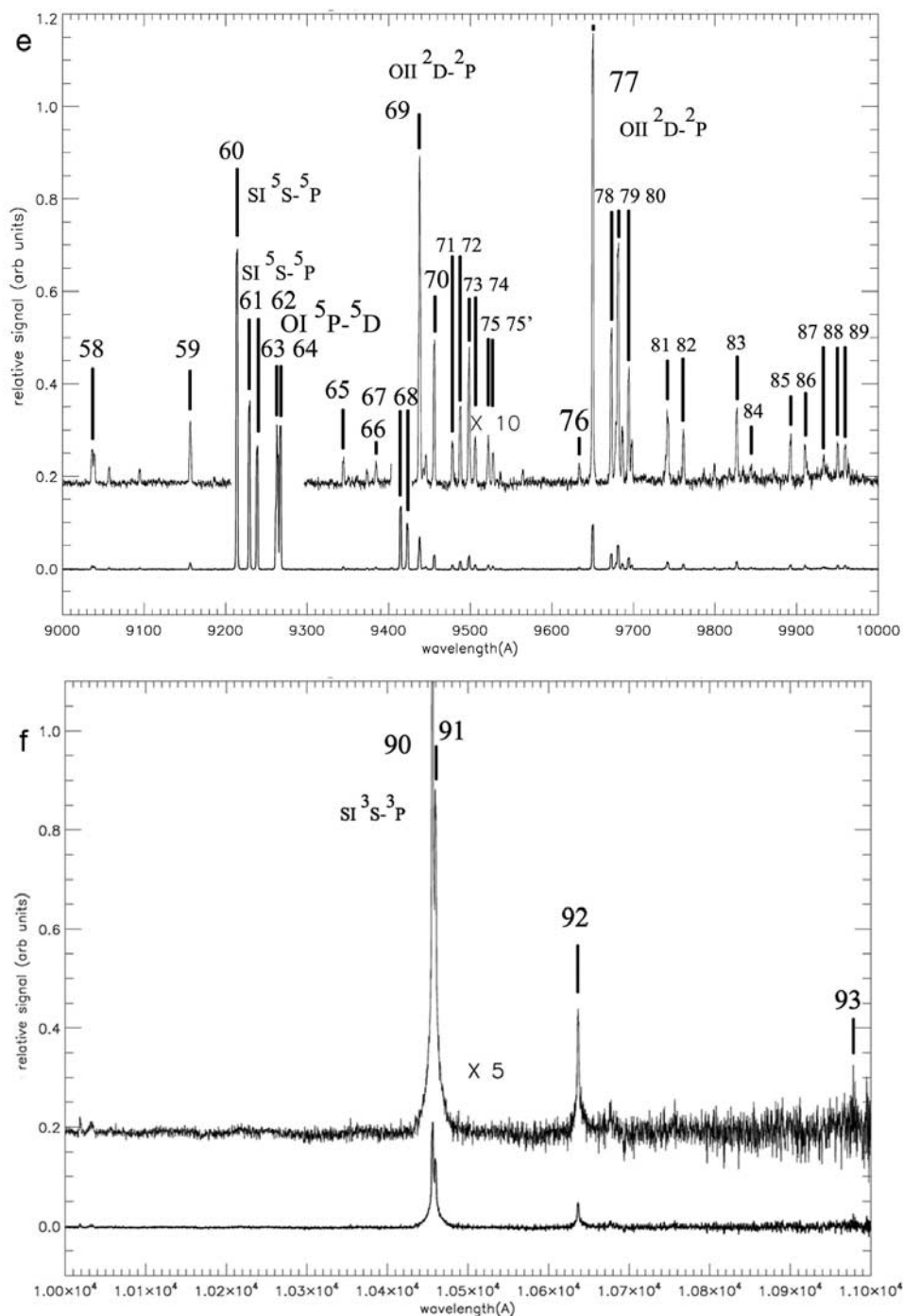


Figure 7. (continued)

emission cross section to be  $3 \times 10^{-19} \text{ cm}^2$  at 25 eV and  $6 \times 10^{-19} \text{ cm}^2$  at 100 eV. Table 2 shows that these same three transitions also have the largest emission cross section at 25 eV electron impact energy.

[18] There are several weak O II and S II multiplets at 100 eV electron impact energy (see Table 2), each with correspondingly low cross sections ( $10^{-20}$ – $10^{-21} \text{ cm}^2$ ) in the wavelength range 6000–11,000 Å. The strongest

unambiguous ion feature listed as 75 is the SII multiplet at 9521.1 Å with a cross section of  $2.43 \times 10^{-20} \text{ cm}^2$  at 100 eV. We find the total cross section at 100 eV for grating 3 from 5700 to 11,000 Å to be  $17.62 \times 10^{-18} \text{ cm}^2$ , with over 90% of the cross section arising from neutral atom multiplets. Correspondingly, we find the total cross section at 25 eV for grating 3 to be  $2.9 \times 10^{-18} \text{ cm}^2$ . The total cross section

**Table 1.**  $e + \text{SO}_2$  Visible Optical Near-Infrared (VOIR) Emission Cross Sections for 4000–6000 Å at 25 eV and 100 eV Measured With Grating 2<sup>a</sup>

Peak Number	100 eV Integrated Cross Section (10 <sup>-20</sup> cm <sup>2</sup> )	25 eV Integrated Cross Section (10 <sup>-20</sup> cm <sup>2</sup> )	Species	Multiplet	NIST Wavelength, Å
0	2.08	–	O I	3s <sup>5</sup> S–4p <sup>5</sup> P	3947.38, 7.48, 7.58
1	0.62	–	S II	4p <sup>4</sup> D–4d <sup>4</sup> F	4145.06
			S II	4p <sup>2</sup> F–4d <sup>2</sup> F	4146.91
2	1.52	–	S I	4s <sup>3</sup> S–4p <sup>3</sup> P	4152.60
			O II	3p <sup>4</sup> P–3d <sup>4</sup> P	4153.30,
3	1.81	–	S II	4p <sup>4</sup> D–4d <sup>4</sup> F	4162.66
4	1.30	–	S II	4p <sup>2</sup> F–4d <sup>2</sup> G	4174.00, 5.26
5	3.00	–	S II	3d <sup>2</sup> F–4f <sup>2</sup> [3]	4369.93
6	1.36	–	S II	4p <sup>4</sup> D–5s <sup>4</sup> P	4463.58
				3d <sup>2</sup> F– <sup>2</sup> [5]	4464.43
7	1.01	–	S II	4s <sup>2</sup> D–4p <sup>2</sup> P	4524.94
8	3.10	1.27	S I	4s <sup>5</sup> S–5p <sup>5</sup> P	4694.13, 5.45, 6.25
9	1.29	–	O II	4p <sup>4</sup> D–6s <sup>4</sup> P	4773.78
				3p <sup>2</sup> D–3d <sup>4</sup> P	4774.08
10	1.55	–	S II	4s <sup>4</sup> P–4p <sup>4</sup> S	4815.55
11	2.33	–	S II	4s <sup>4</sup> P–4p <sup>4</sup> P	4925.34
12	2.37	0.34	O I	3p <sup>5</sup> P–6d <sup>5</sup> D	4968.79
13	2.57	–	S II	4s <sup>2</sup> P–4p <sup>2</sup> P	5014.07
14	1.68	–	S II	3d <sup>2</sup> P–4p <sup>2</sup> S	5027.22
15	2.86	–	S II	4s <sup>4</sup> P–4p <sup>4</sup> P	5032.45
16	1.20	–	S II	4s <sup>2</sup> D–4p <sup>2</sup> D	5201.39
17	2.25	–	S II	4s <sup>2</sup> D–4p <sup>2</sup> D	5212.62
18	2.26	0.90	S I	4s <sup>3</sup> S–5p <sup>3</sup> P	5279.00
19	4.31	–	S II	4p <sup>2</sup> D–4d <sup>2</sup> D	5322.20
20	7.16	0.84	O I	3p <sup>5</sup> P–5d <sup>5</sup> D	5330.74
21	3.27	–	S II	4s <sup>2</sup> D–4p <sup>2</sup> F	5345.72
22	1.35	–	S II	4s <sup>4</sup> P–4p <sup>4</sup> D	5428.67
23	3.47	–	S II	4s <sup>4</sup> P–4p <sup>4</sup> D	5432.81
24	6.93	–	S II	4s <sup>4</sup> P–4p <sup>4</sup> D	5453.83
25	1.92	–	S II	4p <sup>2</sup> D–3d <sup>2</sup> D	5475.01
26	2.25	–	S II	4s <sup>4</sup> P–4p <sup>4</sup> D	5509.72
27	2.10	–	S II	3d <sup>4</sup> F–4p <sup>4</sup> D	5606.15
28	6.68	–	S II	3d <sup>4</sup> F–4p <sup>4</sup> D	5640.33
29	3.54	–	S II	4p <sup>2</sup> D–3d <sup>2</sup> D	5648.35
30	1.28	–	S II	3d <sup>4</sup> F–4d <sup>4</sup> D	5660.00
31	1.16	–	S II	3d <sup>4</sup> F–4p <sup>4</sup> D	5664.78
32	1.45	0.76	S I	4p <sup>5</sup> P–7d <sup>5</sup> D	5706.10

<sup>a</sup> Total VOIR emission cross section at 100 eV for 3900–5700 Å = 83.03 × 10<sup>-20</sup> cm<sup>2</sup>.

at 100 eV for grating 2 from 3900 to 5700 Å is 83.03 × 10<sup>-20</sup> cm<sup>2</sup>.

#### 4. Discussion

[19] Detailed high-resolution VOIR laboratory studies of SO<sub>2</sub> by electron impact have revealed a large number of multiplets from both S and O as the Grotrian diagrams of S and O show [Bashkin and Stoner, 1975a, 1975b] and the atomic wavelength lists of the NIST Atomic Database ([http://physics.nist.gov/PhysRefData/ASD/lines\\_form.html](http://physics.nist.gov/PhysRefData/ASD/lines_form.html)) indicate. The threshold energy for electron dissociative excitation is 15–20 eV [Ajello et al., 1992a]. There are two types of electron distributions at Io, a low-energy 5- to 10-eV thermal component [Saur et al., 2003] and a non-thermal field-aligned tail component [Oliveresen et al., 2001] ~30 eV based on fluctuations in the plasma torus electron flux. The nonthermal electron flux would contribute to the Io emissions for the strong features observed in this study. Higher-energy (keV) electrons are also trapped in the Jovian magnetosphere but their cross sections for exciting emission by impact are far smaller.

[20] In addition to excitation by magnetospheric electron impact, emission from S and O can be excited by solar EUV radiation and photoelectrons. Measuring the change in Io's FUV emission flux in lines of O I and S I between 1250 Å and 1500 Å as Io was eclipsed by Jupiter's shadow, Clarke et al. [1994] found that about two-thirds of the total emission in sunlight was excited by solar EUV (at these wavelengths, Io's diffusely reflected solar spectrum is negligible). This includes the O I multiplets at 1304 Å and 1356 Å that originate from the final levels of the brighter VOIR features reported here; namely, 8446.7 Å and 7773.4 Å, respectively. Electron impact excitation dominates on Io's night side and when Io is in Jupiter's shadow. The results reported here will be useful for modeling Io's emission whether on the sunlit or night hemisphere, but the solar EUV excitation may have to be included in modeling the dayside VOIR emission.

[21] Spacecraft are required in order to view Io's night side, which has been observed by Galileo and the flyby of Cassini and NH spacecraft. Done at different orbital phases, such observations can map all Io longitudes and over a much wider range of wavelengths than is possible from the

**Table 2.**  $e + \text{SO}_2$  VOIR Emission Cross Sections for 5800–11,000 Å at 25 eV and 100 eV Measured With Grating 3<sup>a</sup>

Peak Number	100 eV Integrated Cross Section (10 <sup>-20</sup> cm <sup>2</sup> )	25 eV Integrated Cross Section (10 <sup>-20</sup> cm <sup>2</sup> )	Species	Multiplet	NIST Wavelength, Å
1	1.56 × 10 <sup>-20</sup>	3.91 × 10 <sup>-21</sup>	S II	4s <sup>2</sup> P–4p <sup>2</sup> D	5819.27
2	3.45 × 10 <sup>-21</sup>	5.12 × 10 <sup>-22</sup>	S I	4p <sup>3</sup> P–8s <sup>5</sup> S	5889.75
3	2.57 × 10 <sup>-20</sup>	1.74 × 10 <sup>-20</sup>	O I	3p <sup>3</sup> P–5d <sup>3</sup> D	5958.39, 8.58
			S I	4p <sup>3</sup> P–8d <sup>3</sup> D	5959.11, 61.19
4	1.72 × 10 <sup>-20</sup>	1.00 × 10 <sup>-20</sup>	S I	4p <sup>5</sup> P–6d <sup>5</sup> D	6041.92
5	3.10 × 10 <sup>-20</sup>	1.03 × 10 <sup>-20</sup>	S I	4p <sup>5</sup> P–6d <sup>5</sup> D	6046.04
6	4.00 × 10 <sup>-20</sup>	1.71 × 10 <sup>-20</sup>	SI	4p <sup>5</sup> P–6d <sup>5</sup> D	6052.66
7	1.80 × 10 <sup>-19</sup>	2.00 × 10 <sup>-20</sup>	O I	4s <sup>5</sup> P–4d <sup>5</sup> D	6155.74, 6.78, 8.18
8	3.91 × 10 <sup>-20</sup>	1.82 × 10 <sup>-20</sup>	S I	4p <sup>3</sup> P–7d <sup>3</sup> D	6172.77, 3.61, 4.99, 5.82
9	3.02 × 10 <sup>-21</sup>	–			6249.69 <sup>b</sup>
10	2.55 × 10 <sup>-21</sup>	–	O I	?	6256.83
11	4.03 × 10 <sup>-21</sup>	–	O I	?	6261.55
12	2.00 × 10 <sup>-20</sup>	–	S II	3d <sup>4</sup> D–4p <sup>4</sup> P	6286.35
13		–	S II	3d <sup>2</sup> F–4p <sup>2</sup> D	6289.56
14	9.55 × 10 <sup>-21</sup>	–	S II	3d <sup>4</sup> D–4p <sup>4</sup> P	6305.48
14'	1.47 × 10 <sup>-20</sup>	–	S II	3d <sup>2</sup> F–4p <sup>2</sup> D	6312.66
15	6.39 × 10 <sup>-22</sup>	–	S II	3d <sup>4</sup> D–4p <sup>4</sup> P	6384.89
16	9.81 × 10 <sup>-21</sup>	–	S I	4p <sup>3</sup> P–8s <sup>3</sup> S	6396.08, 6.64
			S II	3d <sup>4</sup> D–4p <sup>4</sup> P	6397.36, 7.99
17	4.08 × 10 <sup>-21</sup>	–	S I	4p <sup>5</sup> P–7s <sup>5</sup> S	6403.58
18	6.95 × 10 <sup>-21</sup>	–	S I	4p <sup>5</sup> P–7s <sup>5</sup> S	6408.13
19	1.03 × 10 <sup>-20</sup>	2.66 × 10 <sup>-21</sup>	S I	4p <sup>5</sup> P–7s <sup>5</sup> S	6415.50
20	7.54 × 10 <sup>-20</sup>	5.89 × 10 <sup>-20</sup>	O I	3p <sup>5</sup> P–5s <sup>5</sup> S	6453.60, 4.44, 5.98
21	3.67 × 10 <sup>-20</sup>	1.57 × 10 <sup>-20</sup>	S I	4p <sup>3</sup> P–6d <sup>3</sup> D	6538.57
22	2.11 × 10 <sup>-20</sup>	–	S I	4p <sup>5</sup> P–5d <sup>5</sup> D	6743.58
23	3.75 × 10 <sup>-20</sup>	1.37 × 10 <sup>-20</sup>	S I	4p <sup>5</sup> P–5d <sup>5</sup> D	6748.79
24	5.17 × 10 <sup>-20</sup>	1.93 × 10 <sup>-20</sup>	S I	4p <sup>5</sup> P–5d <sup>5</sup> D	6757.16
25	4.85 × 10 <sup>-21</sup>	–	O II	3d <sup>2</sup> P–4p <sup>2</sup> D	6856.56
26	7.97 × 10 <sup>-21</sup>	1.17 × 10 <sup>-21</sup>			6860.22, 1.30, 2.46 <sup>b</sup>
27	9.08 × 10 <sup>-21</sup>	–	S II	3d <sup>4</sup> D–4p <sup>4</sup> D	6981.40
28	4.92 × 10 <sup>-21</sup>	1.05 × 10 <sup>-21</sup>			6984.17, 5.13, 6.22 <sup>b</sup>
29	2.64 × 10 <sup>-20</sup>	4.88 × 10 <sup>-22</sup>	O I	3p <sup>3</sup> P–4d <sup>3</sup> D	7001.92
30	7.81 × 10 <sup>-21</sup>	3.73 × 10 <sup>-22</sup>	S I	3d <sup>5</sup> D–8f <sup>5</sup> F	7161.43
31	1.31 × 10 <sup>-20</sup>	2.46 × 10 <sup>-21</sup>	O II	3d <sup>4</sup> D–4p <sup>4</sup> D	7167.83
32	4.52 × 10 <sup>-20</sup>	1.16 × 10 <sup>-20</sup>	S I	4p <sup>3</sup> P–5d <sup>3</sup> D	7242.54, 3.05, 3.74, 4.75
33	1.57 × 10 <sup>-20</sup>	1.77 × 10 <sup>-21</sup>	O I	3p <sup>3</sup> P–5s <sup>3</sup> S	7254.15, 4.45, 4.53
34	2.68 × 10 <sup>-20</sup>	4.16 × 10 <sup>-21</sup>	S I	3d <sup>5</sup> D–7f <sup>5</sup> F	7443.35
35	4.71 × 10 <sup>-20</sup>	6.83 × 10 <sup>-21</sup>			7446.92
36	1.20 × 10 <sup>-20</sup>	–	S II	3d <sup>2</sup> G–4p <sup>2</sup> F	7578.91
36'	6.54 × 10 <sup>-21</sup>	1.05 × 10 <sup>-21</sup>	O II	4p <sup>2</sup> D–4d <sup>2</sup> P	7585.74
36''	8.95 × 10 <sup>-21</sup>	4.24 × 10 <sup>-22</sup>	O II	3d <sup>4</sup> P–4p <sup>4</sup> D	7593.00
36'''	1.05 × 10 <sup>-20</sup>	1.70 × 10 <sup>-21</sup>	O II	3d <sup>4</sup> D–4p <sup>4</sup> D	7599.22, 7602.81
36''''	1.08 × 10 <sup>-20</sup>	1.08 × 10 <sup>-21</sup>	O II	3d <sup>2</sup> F–4p <sup>4</sup> D	7627.46, 8.47
			S II	3d <sup>2</sup> G–4p <sup>2</sup> F	7629.74
37	1.85 × 10 <sup>-20</sup>	3.56 × 10 <sup>-21</sup>	S I	4p <sup>3</sup> P–6s <sup>5</sup> S	7679.61
38	2.53 × 10 <sup>-20</sup>	2.13 × 10 <sup>-21</sup>	S I	4p <sup>5</sup> P–6s <sup>5</sup> S	7686.11
39	4.45 × 10 <sup>-20</sup>	9.36 × 10 <sup>-21</sup>	S I	4p <sup>3</sup> P–6s <sup>5</sup> S	7696.72
40	4.20 × 10 <sup>-18</sup>	3.90 × 10 <sup>-19</sup>	O I	3s <sup>5</sup> S–3p <sup>5</sup> P	7771.94, 4.17, 5.39
41	3.44 × 10 <sup>-20</sup>	6.47 × 10 <sup>-21</sup>	S I	3d <sup>3</sup> D–6f <sup>5</sup> F	7923.84
42	5.37 × 10 <sup>-20</sup>	1.08 × 10 <sup>-20</sup>	S I	3d <sup>5</sup> D–6f <sup>5</sup> F	7927.94
			S II	4p <sup>2</sup> P– <sup>2</sup> P	7928.60
43	2.81 × 10 <sup>-20</sup>	5.71 × 10 <sup>-21</sup>	S I	4p <sup>3</sup> P–4s <sup>3</sup> P	8133.01
44	3.87 × 10 <sup>-20</sup>	8.80 × 10 <sup>-21</sup>	S I	4s <sup>3</sup> D–7p <sup>3</sup> P	8147.81
45	2.77 × 10 <sup>-20</sup>	–	O I	3s <sup>3</sup> D–3p <sup>3</sup> D	8221.82
46	1.55 × 10 <sup>-20</sup>	–	O I	3s <sup>3</sup> D–3p <sup>3</sup> D	8233.00
47	1.72 × 10 <sup>-20</sup>	–	S II	4s <sup>2</sup> P–4p <sup>2</sup> S	8314.59
48	2.60 × 10 <sup>-18</sup>	2.15 × 10 <sup>-19</sup>	O I	3s <sup>3</sup> S–3p <sup>3</sup> P	8446.36
49	1.87 × 10 <sup>-19</sup>	4.24 × 10 <sup>-20</sup>			8585.72 <sup>b</sup>
49'	2.54 × 10 <sup>-20</sup>	4.55 × 10 <sup>-21</sup>	S I	4s <sup>3</sup> D–4p <sup>3</sup> P	8633.23
50	1.47 × 10 <sup>-19</sup>	4.02 × 10 <sup>-20</sup>	S I	4s <sup>3</sup> D–4p <sup>3</sup> P	8668.49
			S I	4p <sup>5</sup> P–4d <sup>5</sup> D	8670.22, 0.65
51	1.87 × 10 <sup>-19</sup>	5.24 × 10 <sup>-20</sup>	S I	4p <sup>5</sup> P–4d <sup>5</sup> D	8679.00, 9.65, 80.46
52	2.52 × 10 <sup>-19</sup>	7.46 × 10 <sup>-20</sup>	S I	4p <sup>5</sup> P–4d <sup>5</sup> D	8693.24, 4.00, 4.71
53	1.25 × 10 <sup>-19</sup>	8.37 × 10 <sup>-22</sup>	O I	3s <sup>1</sup> D–3p <sup>1</sup> F	8820.43
53'	1.48 × 10 <sup>-20</sup>	2.12 × 10 <sup>-21</sup>	S I	4s <sup>3</sup> D–5f <sup>5</sup> F	8833.47
53''	2.36 × 10 <sup>-20</sup>	3.07 × 10 <sup>-21</sup>	S I	4s <sup>3</sup> D–5f <sup>5</sup> F	8847.28
54	1.15 × 10 <sup>-19</sup>	1.93 × 10 <sup>-20</sup>	S I	3d <sup>3</sup> D–5f <sup>5</sup> F	8874.53
55	2.02 × 10 <sup>-19</sup>	3.39 × 10 <sup>-20</sup>	S I	3d <sup>5</sup> D–5f <sup>5</sup> F	8879.62, 80.71, 82.50
56	2.48 × 10 <sup>-20</sup>	3.80 × 10 <sup>-21</sup>			8970.90 <sup>b</sup>
57	2.49 × 10 <sup>-20</sup>	3.47 × 10 <sup>-21</sup>			8977.94 <sup>b</sup>

Table 2. (continued)

Peak Number	100 eV Integrated Cross Section (10 <sup>-20</sup> cm <sup>2</sup> )	25 eV Integrated Cross Section (10 <sup>-20</sup> cm <sup>2</sup> )	Species	Multiplet	NIST Wavelength, Å
58	3.45 × 10 <sup>-20</sup>	9.09 × 10 <sup>-21</sup>	S I	4p <sup>3</sup> P–4d <sup>3</sup> D	9035.92, 6.32, 6.73, 8.72
59	3.82 × 10 <sup>-20</sup>	–	O I	?	9156.01
60	1.80 × 10 <sup>-18</sup>	3.63 × 10 <sup>-19</sup>	S I	4s <sup>5</sup> S–4p <sup>5</sup> P	9212.86
61	9.21 × 10 <sup>-19</sup>	1.76 × 10 <sup>-19</sup>	S I	4s <sup>5</sup> S–4p <sup>5</sup> P	9228.09
62	6.78 × 10 <sup>-19</sup>	1.24 × 10 <sup>-19</sup>	S I	4s <sup>5</sup> S–4p <sup>5</sup> P	9237.54
63	8.10 × 10 <sup>-19</sup>	7.81 × 10 <sup>-21</sup>	O I	3p <sup>5</sup> P–3d <sup>5</sup> D	9260.81, 2.58, 5.94
64	6.70 × 10 <sup>-19</sup>	2.70 × 10 <sup>-20</sup>	O I	3p <sup>5</sup> P–3d <sup>5</sup> D	9265.94, 6.01
65	1.53 × 10 <sup>-20</sup>	–			9343.06 <sup>b</sup>
66	1.40 × 10 <sup>-20</sup>	–			9383.60 <sup>b</sup>
67	3.47 × 10 <sup>-19</sup>	8.27 × 10 <sup>-20</sup>	S I	4s <sup>3</sup> D–4p <sup>3</sup> F	9413.46
			O II	4d <sup>4</sup> P–5f <sup>2</sup> [3]	9417.72
68	2.55 × 10 <sup>-19</sup>	3.52 × 10 <sup>-20</sup>	O II	4d <sup>4</sup> P–5f <sup>2</sup> [1]	9421.49
			S I	4s <sup>3</sup> D–4p <sup>3</sup> F	9421.93
69	1.74 × 10 <sup>-19</sup>	2.31 × 10 <sup>-20</sup>	S I	4s <sup>3</sup> D–4p <sup>3</sup> F	9437.11
70	8.44 × 10 <sup>-20</sup>	9.40 × 10 <sup>-21</sup>	S I	3d <sup>5</sup> D–4p <sup>3</sup> F	9455.43
71	2.94 × 10 <sup>-20</sup>	2.45 × 10 <sup>-21</sup>	S I	3d <sup>5</sup> D–4p <sup>3</sup> F	9477.87
72	4.37 × 10 <sup>-20</sup>	8.92 × 10 <sup>-22</sup>	O I	?	9487.43
73	7.51 × 10 <sup>-20</sup>	8.34 × 10 <sup>-22</sup>	O I	?	9497.97
74	2.16 × 10 <sup>-20</sup>	–	S II	4f <sup>2</sup> [3]–5g <sup>2</sup> [4]	9505.50
			O I	?	9505.59
75	2.43 × 10 <sup>-20</sup>	–	S II	4f <sup>2</sup> [5]–5g <sup>2</sup> [6]	9521.13
75'	1.79 × 10 <sup>-20</sup>	–	S II	4f <sup>2</sup> [3]–5g <sup>2</sup> [4]	9527.58
76	1.52 × 10 <sup>-20</sup>	–	S I	4s <sup>3</sup> D–4p <sup>3</sup> D	9633.13
77	3.14 × 10 <sup>-20</sup>	6.32 × 10 <sup>-20</sup>	O I	4s <sup>3</sup> D–4p <sup>3</sup> D	9649.57
78	8.72 × 10 <sup>-20</sup>	6.02 × 10 <sup>-21</sup>	S I	4s <sup>3</sup> D–4p <sup>3</sup> D	9672.28, 2.53
79	1.59 × 10 <sup>-19</sup>	4.18 × 10 <sup>-20</sup>	S I	4s <sup>3</sup> D–4p <sup>3</sup> D	9680.56
80	9.29 × 10 <sup>-20</sup>	1.95 × 10 <sup>-20</sup>	O I	4s <sup>5</sup> S–6p <sup>5</sup> P	9694.66
81	5.67 × 10 <sup>-20</sup>	5.80 × 10 <sup>-21</sup>	O I	?	9741.50
82	1.34 × 10 <sup>-20</sup>	–	O I	?	9760.65
83	5.09 × 10 <sup>-20</sup>	4.60 × 10 <sup>-21</sup>	O I	3d <sup>5</sup> D–7f <sup>5</sup> F	9826.09
84	1.82 × 10 <sup>-20</sup>	–			9842.36 <sup>b</sup>
85	3.25 × 10 <sup>-20</sup>	–	O I	3d <sup>5</sup> D–7f <sup>3</sup> F	9891.65, 1.72, 1.80
86	3.66 × 10 <sup>-20</sup>	5.27 × 10 <sup>-21</sup>	S I	4s <sup>3</sup> D–6p <sup>3</sup> P	9909.70
87	2.60 × 10 <sup>-20</sup>	4.80 × 10 <sup>-21</sup>	S I	4s <sup>3</sup> D–6p <sup>3</sup> P	9932.36
88	2.37 × 10 <sup>-20</sup>	1.14 × 10 <sup>-21</sup>	S I	4s <sup>3</sup> D–6p <sup>3</sup> P	9949.83
89	3.78 × 10 <sup>-20</sup>	7.34 × 10 <sup>-22</sup>	S I	4s <sup>3</sup> D–4p <sup>1</sup> P	9958.86
90	7.97 × 10 <sup>-20</sup>	3.78 × 10 <sup>-23</sup>	S I	4s <sup>3</sup> S–4p <sup>3</sup> P	10,455.45, 6.76
91	1.06 × 10 <sup>-18</sup>	4.42 × 10 <sup>-19</sup>	S I	4s <sup>3</sup> S–4p <sup>3</sup> P	10,459.41
92	3.53 × 10 <sup>-19</sup>	4.84 × 10 <sup>-20</sup>	S I	4s <sup>1</sup> D–4p <sup>1</sup> F	10,633.08
93	1.02 × 10 <sup>-20</sup>	–	S I	4p <sup>5</sup> P– <sup>3</sup> P	10,955.23

<sup>a</sup>Total VOIR emission cross section at 100 eV for 5700–11,000 Å = 17.62 × 10<sup>-18</sup> cm<sup>2</sup>. Total VOIR emission cross section at 25 eV for 5700–11,000 Å = 2.9 × 10<sup>-18</sup> cm<sup>2</sup>.

<sup>b</sup> Experimentally measured, but not listed in the NIST database.

ground. They are not restricted to the VOIR range; but they could in principle obtain simultaneous FUV and VOIR medium-resolution spectra that compare the S I and O I emission from different excited levels of the cascade to extract additional information about the exciting nonthermal electron energy distribution.

[22] Our measurements of VOIR atomic emissions produced by electron impact on SO<sub>2</sub> raise new questions about previous interpretations of spacecraft observations of Io's atmosphere during the eclipse. *Geissler et al.* [2004] postulated that potassium was responsible for the intense (~20 kR) equatorial emissions detected by the Cassini imaging system in the wavelength range from 7300 Å to 8000 Å. In their model, OI emission at 7773.4 Å caused by electron excitation of O was accounted for, but emission by stimulation of SO<sub>2</sub> was not included. Could the unidentified atmospheric emissions previously attributed to KI D 7665, 7699 Å lines be explained instead by the strong O I multiplet produced by dissociative excitation of SO<sub>2</sub>? We can constrain the intensity of Io's 7773.4 Å OI emission in two ways. Firstly, we expect the intensity of 7773.4 Å to be related to

the intensity of FUV emissions at 1356 Å. These two transitions are both involved in the same cascade path. Independent measurements of the 1356 Å intensity [e.g., *Roesler et al.*, 1999] thus form one constraint on the near-infrared O I emission intensity. Secondly, we can make use of the results of *Geissler et al.* [2004, Table 5] to estimate the intensity based upon the newly derived cross section for 7773.4 Å O I emission produced by dissociative excitation of SO<sub>2</sub>. Both approaches predict emission intensities less than 2 kR, insufficient to account for the near-infrared emissions observed by Cassini. Another species, perhaps K, is still required by the observations.

[23] Earthbound observations are restricted to wavelengths above 3000 Å owing to the opacity of ozone in the Earth's atmosphere, so Io's FUV/UV emission is accessible only from a spacecraft or an Earth-orbiting satellite. However, Io's VOIR spectrum is accessible to ground-based telescopes, and can be resolved spatially over Io's 1" diameter disk through adaptive optics.

[24] There are several particularly strong multiplets of O I and S I that emit in the VOIR and are suitable for ground-

based studies. S I is particularly suitable since there is no blending with telluric airglow features. The strongest S I feature is the  $4s\ ^5S-4p\ ^5P$  multiplet at 9212.87 Å. The ratio of S I to S II or O II features (also found in the 9000–10,000 Å wavelength region) is a convenient electron thermometer. However, the two strongest features in the VOIR spectrum are O I multiplets  $3s\ ^5S-3p\ ^5P$  (7773.4 Å) and  $3s\ ^3S-3p\ ^3P$  (8446.7 Å). It is expected that the direct electron excitation of the atomic species S and O will produce a VOIR spectrum that is similar to that produced by dissociative excitation of SO<sub>2</sub>, either in the laboratory or in the Io atmosphere. However, the threshold energies differ by the energy for dissociative excitation into ground state atoms (S + O + O), which is 11 eV. For example we have found this result in the EUV (700–1350 Å) comparing the spectra of e + O [Johnson *et al.*, 2003] and e + O<sub>2</sub> [Ajello and Franklin, 1985].

[25] Earthbound and Earth-orbit observations of Io see only Io's sunlit hemisphere except when Io is in Jupiter's shadow. The cross sections of the brightest VOIR features mentioned are comparable to their FUV counterparts that originate from the VOIR lower levels. Those intensities were measured by Clarke *et al.* [1994] and found to be 1320 R (including a blended S I multiplet) and 1140 R for O 1304 Å and 1356 Å, respectively, in sunlight and 450 R and 300 R in Jupiter shadow. Similar intensities can be expected for the corresponding VOIR features, which have similar cross sections, if the population of these excited levels is comparable. These line intensities are much less than the intensity of Io's diffusely reflected solar continuum in the VOIR spectral range (MegaRayleighs/Å at 6000 Å). It would, thus, appear that ground-based observation of Io's atomic S and O emission in the VOIR spectral region would require that Io be in Jupiter's shadow. A caveat to this, however, is that FUV HST images have shown S I and O I emission to extend up to an Io diameter above the surface [Ballester *et al.*, 1996; Wolven *et al.*, 2001], offering the possibility that refinements in adaptive optics instrumentation may eventually allow ground-based observation of these lines when Io's disk is illuminated. This would allow observation of emission at different longitudes of Io, including geometries with a plume extending beyond the limb. Of course, the solar EUV excitation would have to be taken into account in the analysis in this case.

[26] If the upcoming servicing mission in 2008 is successful, HST will have the capability to obtain spectra in the 0.9–1 μm range where we have obtained the new laboratory spectra presented here. During this servicing mission, an attempt will be made to repair the STIS spectrograph, which can normally obtain spectra matching the resolution and wavelength range reported here. Three current HST instruments can obtain slitless spectra of these multiplets but only at low resolution. These will not be useful for emission that covers or extends beyond Io's disk because Io's 1" diameter smears the spectrum to an effective resolution element of 120 Å, 270 Å, and 410 Å for the Wide Field and Planetary Camera 2, the Near Infrared Camera and Multi-object Spectrometer, and the Advanced Camera for Surveys, respectively. Since ground-based telescopes with slit spectrographs would have much higher spectral resolution than gratings or ramp filters, and thus able to reduce the continuum background, they remain a viable alternative.

[27] The cross sections as a function of electron energy for the strong multiplets will soon be measured in the VOIR with the addition of energy scanning capability synchronized with the CCD camera photon readouts. However, the excitation functions for O I 1304 Å and 1356 Å, measured by Vatti Palle *et al.* [2004] should be a good approximation to the actual excitation function of O I 8446 Å and 7774 Å multiplets (with a small shift in threshold energy of less than 2 eV), respectively, since cascade contributes at least 50% of the UV resonance line emissions. Vatti Palle *et al.* show the ratios of 100 eV to 25 eV cross sections for the UV lines of O I 1304 Å and 1356 Å are 11.9 and 11.4, respectively, while we find the same cross section ratios for the VOIR lines of O I 8446 Å and 7774 Å are 12.1 and 10.8, respectively.

[28] **Acknowledgments.** The laboratory measurements described in this text were carried out at the Jet Propulsion Laboratory, California Institute of Technology. The work was supported by the NASA Planetary Atmospheres (grant NNG04G131G) and NASA Outer Planets Research Program offices. A.A. and R.S.M. acknowledge the support of a NASA Research Associateship while at the Jet Propulsion Laboratory.

## References

- Aguilar, A., J. M. Ajello, R. S. Mangina, G. K. James, P. Geissler, and L. Trafton (2008), Middle UV to near-IR spectrum of electron-excited H<sub>2</sub>: Cross sections and transition probabilities, *Astrophys. J.*, in press.
- Ajello, J. M., and B. Franklin (1985), A study of the extreme ultraviolet spectrum of O<sub>2</sub> by electron impact, *J. Chem. Phys.*, **82**, 2519–2528.
- Ajello, J. M., G. K. James, I. Kanik, and B. O. Franklin (1992a), The complete UV spectrum of SO<sub>2</sub> by electron impact: 1. The vacuum ultraviolet spectrum, *J. Geophys. Res.*, **97**, 10,473–10,500.
- Ajello, J. M., G. K. James, and I. Kanik (1992b), The complete UV spectrum of SO<sub>2</sub> by electron impact: 2. The middle ultraviolet spectrum, *J. Geophys. Res.*, **97**, 10,501–10,512.
- Ajello, J. M., D. L. Hansen, L. W. Beegle, C. A. Terrell, I. Kanik, G. K. James, and O. P. Makarov (2002), Middle ultraviolet and visible spectrum of SO<sub>2</sub> by electron impact, *J. Geophys. Res.*, **107**(A7), 1099, doi:10.1029/2001JA000122.
- Ballester, G. E. (1998), Magnetospheric interactions in the major planets, *Spec. Publ. SP-413*, Eur. Space Agency, Noordwijk, Netherlands.
- Ballester, G. E., *et al.* (1996), Time-resolved observations of Jupiter's far-ultraviolet Aurora, *Science*, **274**, 409–413.
- Bashkin, S., and J. O. Stoner (Eds.) (1975a), *Atomic Energy Levels and Grotrian Diagrams*, vol. 1, *Hydrogen I–Phosphorus XV*, pp. 2–17, North Holland, Amsterdam.
- Bashkin, S., and J. O. Stoner (Eds.) (1975b), *Atomic Energy Levels and Grotrian Diagrams*, vol. 2, *Sulfur I–Titanium XXII*, pp. 158–174, North Holland, Amsterdam.
- Bhardwaj, A., and M. Marykuty (1999a), On the excitation of Io's atmosphere by the photo-electrons: Application of the analytical yield spectral model of SO<sub>2</sub>, *Geophys. Res. Lett.*, **26**, 393–396.
- Bhardwaj, A., and M. Marykuty (1999b), Monte Carlo model for electron degradation in SO<sub>2</sub> gas: Cross section, yield spectra and efficiencies, *J. Geophys. Res.*, **104**, 24,713–24,728.
- Clarke, J. T., J. Ajello, J. Luhmann, N. Schneider, and I. Kanik (1994), Hubble Space Telescope UV spectral observations of Io passing into eclipse, *J. Geophys. Res.*, **99**, 8387–8402.
- Esposito, L., *et al.* (2005), Ultraviolet imaging spectroscopy shows an active Saturnian system, *Science*, **307**, 1251–1255.
- Feaga, L. M., M. A. McGrath, and P. D. Feldman (2002), The abundance of atomic sulfur in the atmosphere of Io, *Astrophys. J.*, **570**, 439–446.
- Geissler, P. E., A. C. McEwen, W. Ip, M. J. S. Belton, T. V. Johnson, W. H. Smyth, and A. P. Ingersoll (1999), Galileo imaging of atmospheric emissions from Io, *Science*, **285**, 870–874.
- Geissler, P., A. McEwen, C. Porco, D. Strobel, J. Soar, J. Ajello, and R. West (2004), Cassini observations of Io's visible aurora, *Icarus*, **172**, 127–140.
- Johnson, P. V., I. Kanik, D. Shemansky, and X. Liu (2003), Electron impact cross sections of atomic oxygen, *J. Phys. B*, **36**, 3203–3218.
- Karolis, C., and E. Harting (1978), Electron impact dissociation cross sections in hydrogen and deuterium leading to balmer alpha and beta emission, *J. Phys. B*, **11**, 357–369.
- Kedzierski, W., C. Malone, and J. W. McConkey (2000), Dissociative excitation of SO<sub>2</sub> by electron impact, *Can. J. Phys.*, **78**, 617–624.

- Kiehling, J. E., T. F. Ammirati, M. D. Moore, M. N. Monce, and E. F. Hansel (2001), Proton impact of SO<sub>2</sub>, *J. Geophys. Res.*, *106*, 26,147–26,154.
- Lavrov, B. P., and A. V. Pipa (2002), Account of fine structure of hydrogen levels in the effective emission cross sections of Balmer lines excited by electron impact in gases and plasmas, *Opt. Spectrosc.*, *92*, 647–657.
- Miller, K., and K. Becker (1987), Ultraviolet and visible fluorescence produced by controlled electron impact on SO<sub>2</sub>, *Can. J. Phys.*, *65*, 530–534.
- Noren, C., I. Kanik, P. V. Johnson, P. McCartney, G. James, and J. Ajello (2001), Electron impact studies on atomic oxygen: II. Emission cross section measurements of the O I <sup>3</sup>S → <sup>3</sup>P transition 130.4 nm, *J. Phys. B*, *34*, 2667–2677.
- Oliveren, J. R., F. Scherb, W. H. Smyth, M. E. Freed, R. C. Woodward Jr., M. L. Marconi, K. D. Retherford, O. L. Lupie, and J. P. Morgenthaler (2001), Sunlit Io atmospheric [O I] 6320 Å emission and plasma torus, *J. Geophys. Res.*, *106*, 26,183–26,194.
- Porco, C., et al. (2003), Cassini imaging of Jupiter's atmosphere, satellites and rings, *Science*, *299*, 1541–1547.
- Retherford, K. D., H. W. Moos, D. F. Strobel, and B. C. Wolven (2000), Io's equatorial spots—Morphology of neutral UV emissions, *J. Geophys. Res.*, *105*, 27,157–27,165.
- Retherford, K. D., H. W. Moos, and D. F. Strobel (2003), Io's auroral limb glow: Hubble Space Telescope FUV observations, *J. Geophys. Res.*, *108*(A8), 1333, doi:10.1029/2002JA009710.
- Retherford, K. D., et al. (2007a), Io's atmospheric response to eclipse: UV aurorae observations, *Science*, *318*, 237–240.
- Retherford, K. D., A. Cheng, H. A. Weaver, J. R. Spencer, D. F. Strobel, and J. Saur (2007b), New Horizons LORRI observations of Io's visible aurora in eclipse, paper presented at Magnetospheres of the Outer Planets Meeting, Space Sci. and Eng., Southwest Res. Inst., San Antonio, Tex., June.
- Retherford, K. D. et al. (2007c), Io eclipse observations during the New Horizons flyby, paper presented at the AAS/DPS Meeting, Univ. of Cent. Fla., Orlando, Oct.
- Roesler, F. L., H. W. Moos, R. J. Oliveren, R. C. Woodward Jr., W. H. Smyth, P. D. Feldman, and D. F. Strobel (1999), Far ultraviolet imaging spectroscopy of Io's atmosphere with HST/STIS, *Science*, *283*, 353–357.
- Saur, J., F. M. Neubauer, D. Strobel, and M. Summers (2000), Io's ultraviolet aurora: Remote sensing of Io's interaction, *Geophys. Res. Lett.*, *27*, 2893–2896.
- Saur, J., A. Pouquet, and W. H. Matthaeus (2003), An acceleration mechanism for the generation of the main auroral oval on Jupiter, *Geophys. Res. Lett.*, *30*(5), 1260, doi:10.1029/2002GL015761.
- Terrell, C. A., D. L. Hansen, and J. M. Ajello (2004), The near-ultraviolet and visible emission spectrum of O<sub>2</sub> by electron impact, *J. Phys. B*, *37*, 1931–1949.
- Vatti Palle, P., J. Ajello, and A. Bhardwaj (2004), High-resolution far ultraviolet spectrum of electron-excited SO<sub>2</sub>, *J. Geophys. Res.*, *109*, A02310, doi:10.1029/2003JA009828.
- Wolven, B. C., H. W. Moos, K. D. Retherford, P. D. Feldman, D. F. Strobel, W. H. Smyth, and F. L. Roesler (2001), Emission profiles of neutral oxygen and sulfur in Io's exospheric corona, *J. Geophys. Res.*, *106*, 26,155–26,182.
- Wong, M. C., and W. H. Smyth (2000), Model calculations for Io's atmosphere at eastern and western elongations, *Icarus*, *146*, 60–74.

A. Aguilar, Advanced Light Source, Lawrence Berkeley National Laboratory, Berkeley, CA 94720, USA.

J. M. Ajello, G. K. James, and R. S. Mangina, Jet Propulsion Laboratory, California Institute of Technology, Pasadena, CA 91109, USA. (geoffrey.james@jpl.nasa.gov)

P. Geissler, U.S. Geological Survey, Flagstaff, AZ 86001, USA.

L. Trafton, Department of Astronomy, University of Texas at Austin, Austin, TX 78712, USA.